Molecular dynamics simulation of ballistic effects in mesoporous silica

Yu Lou, Bertrand Siboulet, Sandrine Dourdain, Mohamed Ruwaid Rafiuddin, Xavier Deschanels, Jean-Marc Delaye

Molecular Dynamics Simulation of Ballistic Effects in Mesoporous Silica

Yu Lou[1], Bertrand Siboulet[1], Sandrine Dourdain[1], Mohamed Ruwaid Rafiuddin[1], Xavier Deschanels[1], Jean-Marc Delaye[*2]

[1]ICSM, CEA, CNRS, ENSCM, Univ Montpellier, Marcoule, France

[2]DE2D, CEA, DES, DE2D, Univ. Montpellier, Marcoule, France

Abstract

Accumulation of ion displacement cascades in mesoporous silica material have been modeled using molecular dynamics (MD). For nuclear energies exceeding 30 keV/nm^3, the volume and structural properties (Si-O-Si bond angle, coordination of O and Si) of the mesoporous silica material are modified thereby resulting in the complete collapse of the structure. Similar results were obtained from Au$^+$ ion-irradiation (E = 0.5 MeV) experiments on mesoporous silica samples in which the density of the samples was shown to increase upon irradiation before saturating at deposited nuclear energies exceeding 30 keV/nm^3. Both ion-irradiation experiments and MD simulations have shown that the ballistic effects are responsible for inducing densification of the mesoporous silica material. The mechanism underlying this densification is discussed in terms of irradiation induced sintering.

Keywords: Mesoporous silica, Molecular Dynamics, Radiation damage, Ion irradiations, Pore collapse

Introduction

Mesoporous silica have attracted a great deal of interest since the pioneering synthesis of M41S materials in the early 90's.[1] Identified first to supplant the traditional molecular sieves having pore sizes of the order of several Å, research on these materials has also been greatly boosted by the milestone SBA family with unprecedented large pores of 5 nm to 30 nm[2]. These large and accessible surface areas which can moreover be functionalized, have opened up numerous routes for applications in adsorption,[3] catalysis,[4] sensing[5] or gas storage.[6]

In the field of nuclear waste conditioning, mesoporous silica are proposed as a promising host matrix for storing radioactive wastes. An innovative and compact process named separation-conditioning has been proposed to both separate and confine radioactive elements with mesoporous silica materials.[7] This process takes advantage of the large accessible internal

---

[*]Corresponding author: jean-marc.delaye@cea.fr

surface of the mesoporous silica to selectively adsorb the radionuclides present in the contaminated effluent. The adsorbed radionuclides can further be confined within the structure via chemical or thermal pore collapse. Furthermore, the mild temperature of the process, compared to those of conventional nuclear glass (around 1200°C) brings new possibilities for the conditioning of volatile radionuclides such as I, Cs. However, once the radionuclides are adsorbed and stored within the matrix, the mesoporous structure is exposed to self-irradiation, thereby affecting the long-term conditioning performance of the material. Self-irradiation could result in the collapse of the structure and hence it is important to evaluate the effect of ion-irradiation on mesoporous structures (silica, zirconia,[8] titania,[9]etc.).

For these reasons, it is important to investigate the behavior of porous material under ionic irradiation by considering factors such as the pore size, structure of the material, and the ion-irradiation conditions (energy of the ions, fluence).

Several experimental studies were carried out using high energetic ions (electronic effect). Klaumünzer[10] irradiated nanoporous Vycor glass mainly composed of amorphous SiO_2 using heavy ions above ion track threshold (dE/dx~2-4 keV/nm). To explain the ion-beam induced compaction, this author proposed a stress relaxation model near hot fluidic tracks. Dourdain et al.[11] irradiated ordered mesoporous silica thin films using Xe 92MeV ions (> track threshold) and observed an open channel morphology as signs of tracks formation. Lou et al.[12] irradiated SBA-15 and MCM-41, two ordered mesoporous silica materials, by Ne 278 MeV (dE/dx<0.9 keV/nm) and Ar 493 MeV (dE/dx~3 keV/nm). It was found that SBA-15 with thicker walls and larger pores are more resistant than MCM-41. Kucheyev et al.[13,14] irradiated porous silica aerogels with several ion beams and observed enhancements of mechanical properties either with (C ion) or without (H, He ions) pore collapse.

In another study, metallic foams (Au, Ag) have been irradiated using low energy ions (Ne-45keV, Kr-800keV) .[15,16] A recent review[17] reports the main conclusions of these works: in situ TEM observations have shown the collapse of the mesoporous foams upon irradiation and reveal that the rate of shrinkage depends on the pore size and irradiation temperature. These experiments have allowed the evaluation of the diffusivities of the defects clusters in nanoporous metals, and the prediction by molecular dynamics simulation of a window of radiation tolerance for nanoporous metals in terms of ligament size and dose rate. This radiation tolerance of nanoporous metal was observed by Bringa et al.[16] and it would be interesting to determine if similar results can be obtained using other materials. The high surface/volume ratio of nanoporous material would mean that the surfaces could act as defect sinks for the annihilation of the radiation-induced defects clusters. Besides, the collapse of the nanoporous structure is observed when the ligaments are thin enough to be directly broken by the cascades. When the ligaments are too thick, the accumulation of defects also leads to the rupture of ligaments. Based on these results, it can be observed that a low defect diffusivity and high dose rate could favor the rupture of ligament.

To the best of our knowledge, very few studies have focused on the behavior of oxides under ionic irradiation in the ballistic regime. In a previous study by Lou et al. [18], the mesoporous silica thin films deposited on silicon wafer was observed to collapse upon ion irradiations (Au – 0.5 MeV). Similarly, irradiation of mesoporous zirconia thin films was shown to induce a shrinkage of the material resulting from the collapse of the mesopores without any loss of crystallinity of the zirconia structure.[19] However, the mechanism leading to the collapse of the mesoporous structure under ballistic irradiation is not fully understood. Several studies based on molecular dynamics simulation attribute the collapse of the structure to sputtering processes in metallic materials[20] and organosilicate glasses.[21]

The main objective of this study is to establish a simulation methodology to determine the level of ballistic damage needed to collapse a mesoporous structure, as well as its influence on the covalent bonding state of the silica network. The results of molecular dynamics calculation were compared with experimental results[18] obtained from Au (0.5 MeV) ion irradiation of mesoporous silica and a mechanism for the evolution of these materials under ballistic damage has been proposed in this study.

Computational and experimental methods

1. Creation of simulation cell

The cell was built following the methods presented in works of Siboulet et al.[22] The objective is to obtain a cell of 9 nm × 11 nm × 6 nm with four cylindrical pores (Ø = 3.5 nm) with cubic symmetry. The shape and dimension were chosen in order to represent the mesoporous silica thin film structure presented in a previous experimental work [12]. The simulation box contains 22800 atoms (Si : O = 1 : 2). To maximize the calculation efficiency, one eighth of the cell called sub-cell containing 1/2 pore was firstly built. Then eight sub-cells were stacked following a periodic condition. To build a sub-cell, a Monte-Carlo (MC) quenching technique in canonical ensemble (NVT) with BKS (Van Beest, Kramer, Van Santen) potential [23] was used. Initially, atoms were homogeneously dispersed in the cell. The cell was artificially heated to 4000 K using a radial repulsive potential to create empty voids corresponding to the pores. The temperature was gradually decreased until 300K using the relation $T_{n+1}= 0.98T_n$ Each temperature comprises at least one million MC trials. The quenching was repeated until the intrinsic defects (Si with 5 first neighbor O atoms, noted Si^V and Non-bridging-oxygen, noted NBO) could not be further removed and until no cavities were visible in the wall. The initial simulation box is shown on Figure 2.a.

2. Simulation of the series of displacement cascades

Several authors simulated irradiation effects on conventional fully densified silica [24,25,26,27,28,29]. However, to the best of our knowledge, the effect of irradiation on mesoporous silica has not been investigated. The method used in the present study is derived from previous works described in the references[28,29].

2.1 Choice of the interaction potentials

The process to simulate irradiations was performed using the DL-POLY_3 Molecular Dynamics pack[30]. At short distance, ZBL (Ziegler, Biersack and Littmark) potentials are applied[31]. The ZBL potentials have been fitted to represent the short-range interactions that can occur during a displacement cascade. At long distance, the BKS potentials[23] are applied. The ZBL and BKS potentials are connected together by polynomial expressions that guarantee the continuity of the energy, force and force derivative. Compaction (or densification) is one of the major effects when irradiating porous materials compared to non-porous ones. To follow the change in the density of the sample during a series of displacement cascades, relaxations in the isothermal isobaric ensemble (NPT) are regularly performed. These relaxations are used to follow the equilibrium volume change, hence the density modification, versus the deposited energy.

2.2 Preparation of the initial structure

3

After the creation of the initial structure by a Monte Carlo method, a relaxation has been applied to eliminate the remaining structural defects. The initial relaxation process is the following: the system is first relaxed at 2000 K during 50 000 steps in the NPT ensemble, then quenched to room temperature at a rate of 2×10^{12} K/s and finally relaxed during another 20 000 steps in the NPT ensemble at room temperature (the volume versus time graph corresponding to this final relaxation is provided in the Supplementary Information). The dimensions of the simulation cell after this initial relaxation are 8.89nm x 10.87nm x 5.93nm in the X, Y and Z directions respectively.

2.3 Simulation of series of displacement cascades

To study the structural response of mesoporous silica to ballistic effects, series of displacement cascades have been simulated. Each series contains 100 individual displacement cascades and a total of 50 series was used to reach the final stationary state.

To initiate the displacement cascades, one Si atom is selected randomly alternatively in the bottom layer (i.e. with a low Z coordinate) and in the upper layer (i.e. with a high Z coordinate) of the simulation cell. This atom is then translated at the center of the (X,Y) plan without modifying its Z coordinate and converted into a pseudo Uranium, U atom by increasing its mass. It means that the mass of a U atom is attributed to this Si atom without any modifications of the interaction potentials. The other atoms are translated with the same vector considering the periodic boundary conditions.
A pseudo Uranium atom with an energy of 1.2 keV was used as a projectile in this simulation. This energy has been selected to confine the volume of the cascade within the simulation box and also to reduce the computational time required to reach the final stationary state within few months of calculations.
The displacement cascades are simulated alternatively from the bottom towards the top of the simulation box, and from the top towards the bottom of the simulation box by accelerating the projectile at an energy of 1.2 keV. This alternation in the acceleration direction has been introduced first to irradiate the structure homogeneously and second to avoid a gradual drift of the simulation box. Indeed, if the accelerations were systematically carried out in the same direction, the average linear momentum of the atoms would increase in one direction.
Each irradiation lasts 80 000 steps. The time step can change during the calculation of a displacement cascade in order to guarantee that an atomic displacement during one time step is systematically lower than 0.05Å.

To decrease the temperature to 300 K at the end of a displacement cascade, the atomic velocities in a 0.3 nm thick layer are regularly rescaled to 300K on the X-Z and Y-Z surfaces and on the X-Y surface at the opposite of the initial projectile location. By this method, the excess kinetic energy introduced by the initial projectile is progressively removed.

The TRIM 2013 code[32] has been used to estimate *a priori* the mean free path of a U projectile inside the mesoporous material (Density, d = 2.2 g/cm^3). The calculated nuclear and electronic stopping powers of the U projectile are 0.48 keV/nm and 0.047 keV/nm, respectively. The stopping powers of the 0.5 MeV Au ions were calculated in a same way ((dE/dx) $_{electronic}$= 0.99keV/nm and (dE/dx)$_{nuclear}$= 3.14kev/nm). The deposited energies presented on Figure 13 has been obtained by multiplying the stopping power by the fluence.

2.4 NPT Relaxations

The displacement cascades are simulated keeping the volume constant, which means that the pressure may change with the accumulation of ballistic effects To avoid an unphysical change of the internal pressure, NPT relaxations are performed after each series of displacement cascades, *i.e.* every 100 individual cascades. The NPT relaxations are performed as follows: first a 20 000 time steps relaxation is calculated in the NPT ensemble at 300 K followed by a 5000 time steps relaxation in the NVE ensemble. After this relaxation, the internal stress significantly decreases. Note that during the NPT relaxation, the three dimensions (Lx, Ly and Lz) are modified in the same proportions to anneal the internal pressure. It corresponds to an isotropic volume change that could introduce a bias in the shrinkage dynamics. We will come back to this point later and in the Supplementary Information.

Evolution of the internal stress $\sigma_{\alpha\alpha}$ (i.e. the component of the stress tensor along the X axis) versus the number of displacement cascades is shown in Figure 1 as an example. One can observe that $\sigma_{\alpha\alpha}$ is annealed after each series of 100 displacement cascades.
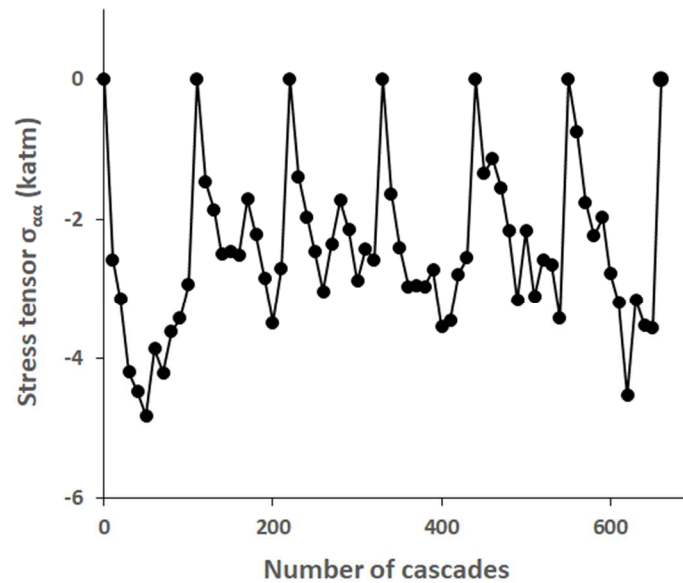

Figure 1. First diagonal component of the stress tensor ($\sigma_{\alpha\alpha}$) versus the number of displacement cascades during the accumulation of series of displacement cascades. After each NPT relaxation (see text), $\sigma_{\alpha\alpha}$ goes back to nearly zero. The $\sigma_{\alpha\alpha}$ negative values during one series of displacement cascades illustrate the contraction trend. Only 6 series of displacement cascades are shown but the trend remains the same for each series.

3. Structural analyses of the irradiated structures

To characterize the pristine and irradiated structures, several means have been used: direct observation, calculation of the changes in the dimension of the cell, and measures of structural characteristics such as the local angles, the Non Bridging Oxygen (NBO) and three coordinated oxygen (O^{III}) concentrations. These analyses have been used previously to characterize structural changes in silica after irradiations.[24,25,26,27,28,29]

To complete these analyses, the quantities of surface and bulk atoms have also been calculated. To do this, a method based on the determination of the local Voronoï volumes was used. As the surface atoms are located near the pores, their local Voronoï volumes are large. To identify the surface atoms, a Monte-Carlo algorithm was used to randomly pick 1 million points in the cell. Then for each atom, the number of points nearest to it than to any other atoms is quantified. By plotting the distribution of these numbers, it has been possible to

determine a threshold: if the number of points around one atom is larger than 60, this atom is considered as a surface one. Note that the threshold depends on the quantity of random points used.

4. Sample Preparation

Mesoporous thin films were dip-coated on silicon substrate <1 0 0>, following the protocol described in reference 18. The method is based on a sol-gel silica template with pluronic P123 surfactant. The thin films (~60 nm) present an hexagonal stacking of cylindrical pores (P6m) with diameters of about 4 nm and a density of 1.1 g/cm^3 corresponding to a relative density of about 50%. The thin films were also heated from 300 to 1000°C in order to compare the structural response of mesoporous silica under irradiation versus thermal treatment.

5. Irradiation conditions

Samples were irradiated using 0.5 MeV Au ions on the Japet accelerator at JANNUS facility at CEA Saclay (France) and the ion beams are oriented in the normal direction with respect to the sample surface. The sample holder was cooled to room temperature during irradiation. The maximum fluence was $1{\times}10^{15}$ Au/cm^2. The flux for all irradiations was fixed at $1{\times}10^{11}$ Au/cm^2.s. Irradiation details are given in ref 18.

6. Thin film characterizations

The mesoporous films were characterized before and after irradiation by XRR measurements performed on a Brucker D8 Advance diffractometer, equipped with a motorised reflectivity stage that allows vertical translation of the sample. The complete primary optics setup for XRR analysis was composed of a Cu Ka (l= 1.54 Å) source, a Göbel mirror, a motorised divergence slit, a fixed 0.2 mm slit, an automatic absorber, a fixed 0.1 mm slit after the absorber, and 2.5° Sollers slits. The secondary optics included a motorised anti-scattering slit, a graphite monochromator, 2.5° Sollers slits, a 0.05 mm receiving slit and a point detector. Standard q-2q scans were used for data collection. The scanning range was from 0° to 5° (2θ) with 0.01°- 3s per step.

Results

1. Simulation of mesoporous structural evolution under irradiation

The direct mesoporous structural evolution as a function of the deposited energy is shown in a series of figures (Figures 2.a to 2.f). Before the accumulation of displacement cascades, the mesopores correspond to cylinders with slightly rough surfaces. A significant shrinkage begins to be visible after the first series of irradiation (Figure 2.b). Then, the pores progressively collapse with the accumulation of the displacement cascades. After 50 series of 100 displacement cascades, the pores are no longer visible. In parallel to the pore shrinkage, the density of the silica increases.
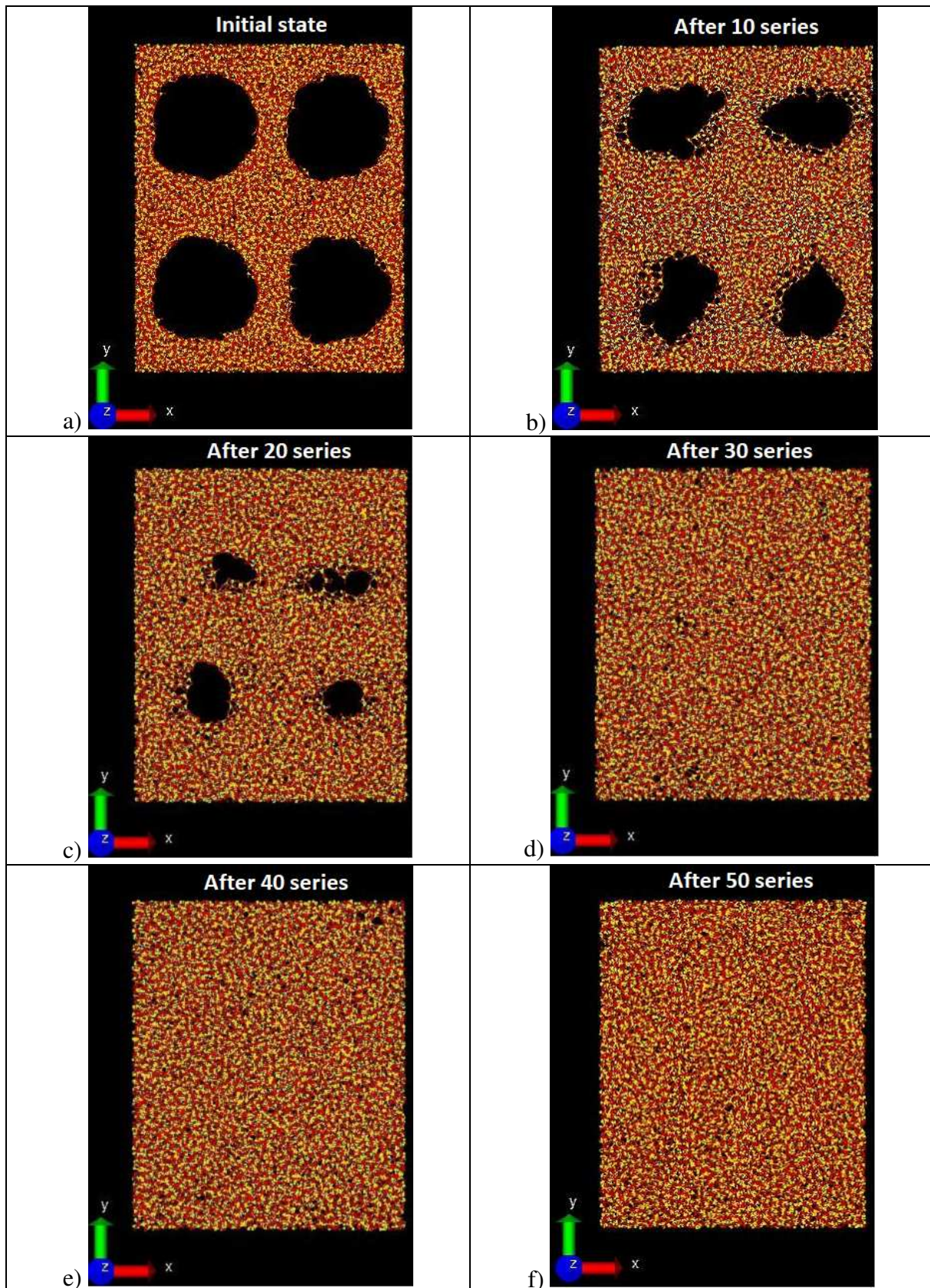
Figure 2: Progressive shrinkage of the porous structure with the accumulation of ballistic effects. a. structure before irradiation, b. after 10 series of 100 displacement cascades, c. after 20 series of 100 displacement cascades, d. after 30 series of 100 displacement cascades, e. after 40 series of 100 displacement cascades, f. after 50 series of 100 displacement cascades.

2. Stress tensor change

As mentioned in the Section 2.4, each relaxation in the NPT ensemble after a series of 100 displacement cascades is isotropic i.e. the same contraction is applied along the X, Y and Z axis to remove the internal pressure. Nevertheless, the stress could not be identical in the three directions. In order to verify this, the diagonal elements of the stress tensor (called $\sigma_{\alpha\alpha}$, $\sigma_{\beta\beta}$ and $\sigma_{\gamma\gamma}$) have been plotted on Figure 3. The values have been taken at the end of a 100 displacement cascade series before the relaxation in the NPT ensemble.

The value of the stress tensor along the different components (absolute value) was found to increase with the deposited energy for the first 20 series, before decreasing beyond 20 series. The radiation effect on the tensile stress is then nonlinear and a maximum is observed at an intermediate stage. It could be linked to the shrinkage of the material during the accumulation of displacement cascades. An acceleration of the shrinkage after the first series of displacement cascades could explain the observation of negative slope at the beginning. At the end, the structure reaches a new metastable state, and the radiation effect on the tensile stress decreases. This observation will be correlated to the density and structural changes after irradiation and will be discussed in the later sections of this article. Figure 3 confirms that the pores have completely disappeared after 50 series of 100 displacement cascades and that a new metastable state has been reached.

It can be seen also that the $\sigma_{\alpha\alpha}$ component tends to be slightly lower (in absolute value) compared to the two others, even if the difference remains small. The dissymmetry of the calculations could be explained by the fact that the cylindrical pores are aligned along the z direction, and the projectiles are accelerated along the y direction. So, the x direction is perpendicular both to the pore axis and to the acceleration direction. But this dissymmetry could also be due to the fact that an isotropic NPT relaxation is applied after each series of 100 displacement cascades while the simulation cell is not isotropic. In fact, as shown in the Supplementary Information (Figures 2 and 3), a slight dissymmetry is introduced on the diagonal terms of the stress tensors before a series of displacement cascades especially during the first 20 series.
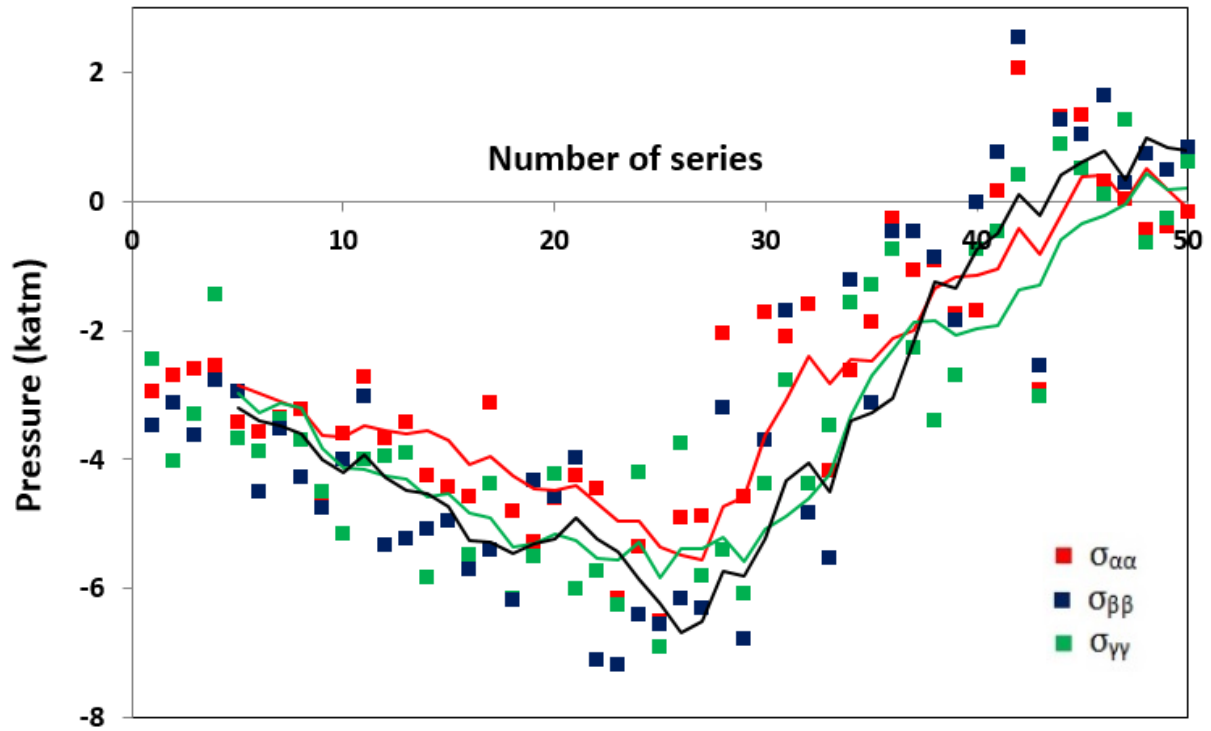
Figure. 3. The σ$_{αα}$, σ$_{ββ}$ and σ$_{γγ}$ components of the stress tensor at the end of each series of 100 displacement cascades (50 series) before the relaxation in the NPT ensemble. The lines correspond to 5-data moving average.

3. Location of the atoms with a large local free volume

The surface atoms are identified by using the method based on the knowledge of the local Voronoï volumes. The locations of the surface atoms after 0, 10, 20, 30, 40 and 50 series of 100 displacement cascades are plotted in Figure 4.

This method is not able to completely separate the atoms at the surface of the mesopores from the bulk atoms with a large local free volume. Therefore, it can be seen that in the initial configuration, some atoms are found quite far from the surfaces of the mesopores. These atoms can be considered as intrinsic defects.

The surface atoms are practically only oxygen (red spheres in Figure 4). Very few Si atoms have been detected (yellow spheres in Figure 4). The progressive extinction of the mesopores with the accumulation of displacement cascades is clearly seen. Beyond 30 series of displacement cascades, the mesopores are not visible indicating a collapse of the pore structure.
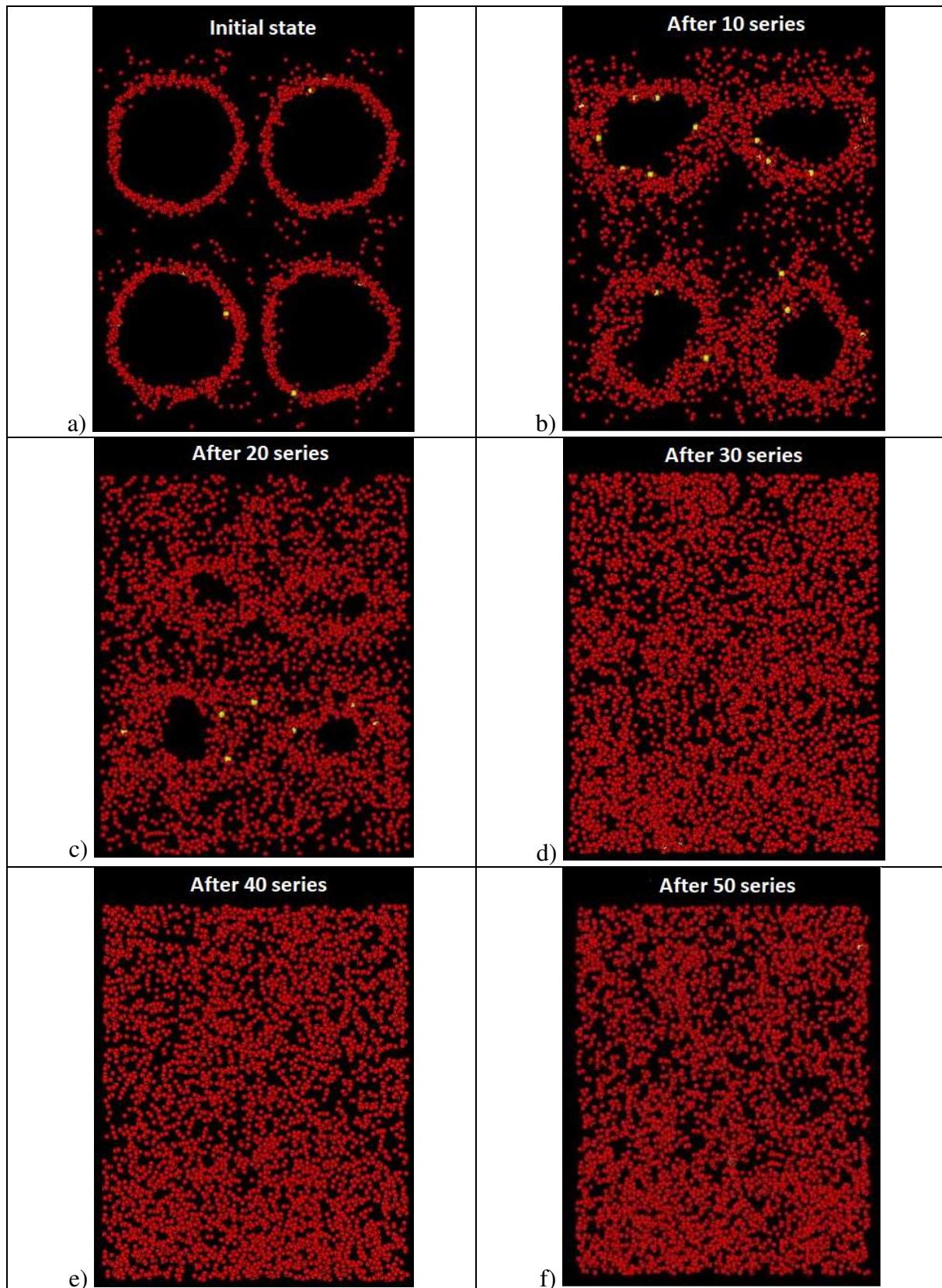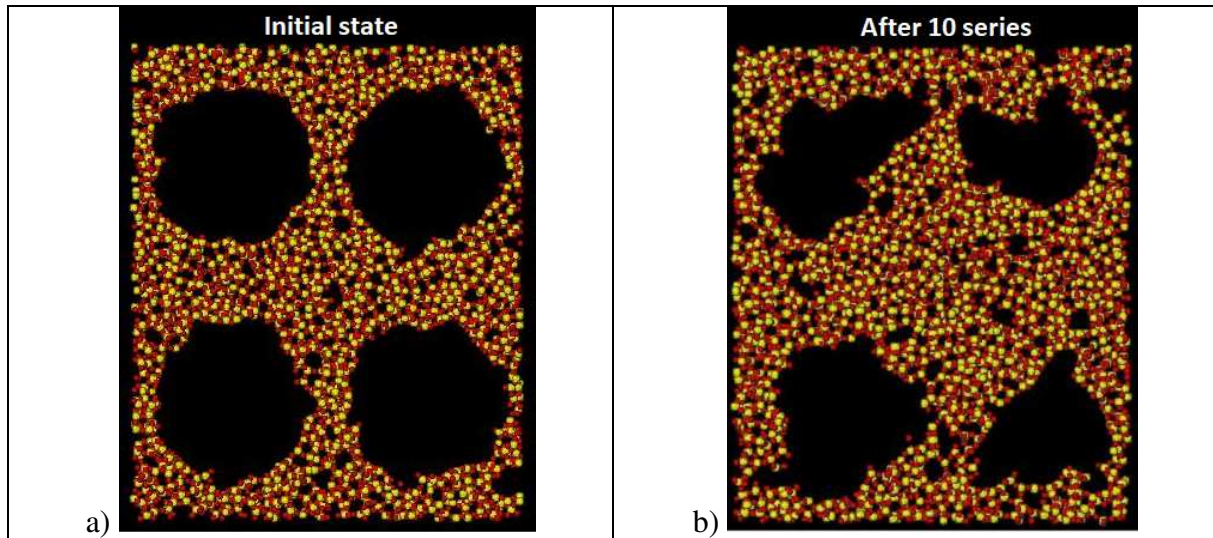
Figure 4: Location of the atoms with a large local free volume (see definition in text). a. before irradiation, b. after 10 series of 100 displacement cascades, c. after 20 series of 100 displacement cascades, d. after 30 series of 100 displacement cascades, e. after 40 series of 100 displacement cascades, f. after 50 series of 100 displacement cascades.

Number of series	Total number	O	Si
0	2169	2160	9
10	2605	2587	18
20	3282	3274	8
30	4186	4184	2
40	4080	4080	0
50	4065	4063	2

Table I: Total number of atoms with a large local free volume (see definition in the text). The respective numbers of O and Si atoms are also indicated.

However, in spite of the extinction of mesopores , the number of atoms characterized by a large local free volume increases continuously with the deposited energy up to 30 series of 100 displacement cascades before stabilization in the number of atoms after 30 series. (See Table I). It means that a significant free volume is created inside the bulk in parallel to the shrinkage of the initial mesopores until a stationary state is reached.

To confirm the creation of free volume within the bulk of the material, 10 Å thick slides in the initial configuration and after 10, 20, 30, 40 and 50 series of 100 displacement cascades have been plotted in Figure 5. With the disappearance of mesopores, there is a simultaneous increase in the formation of larger rings within the bulk of the material beyond 30 series of displacement cascades.
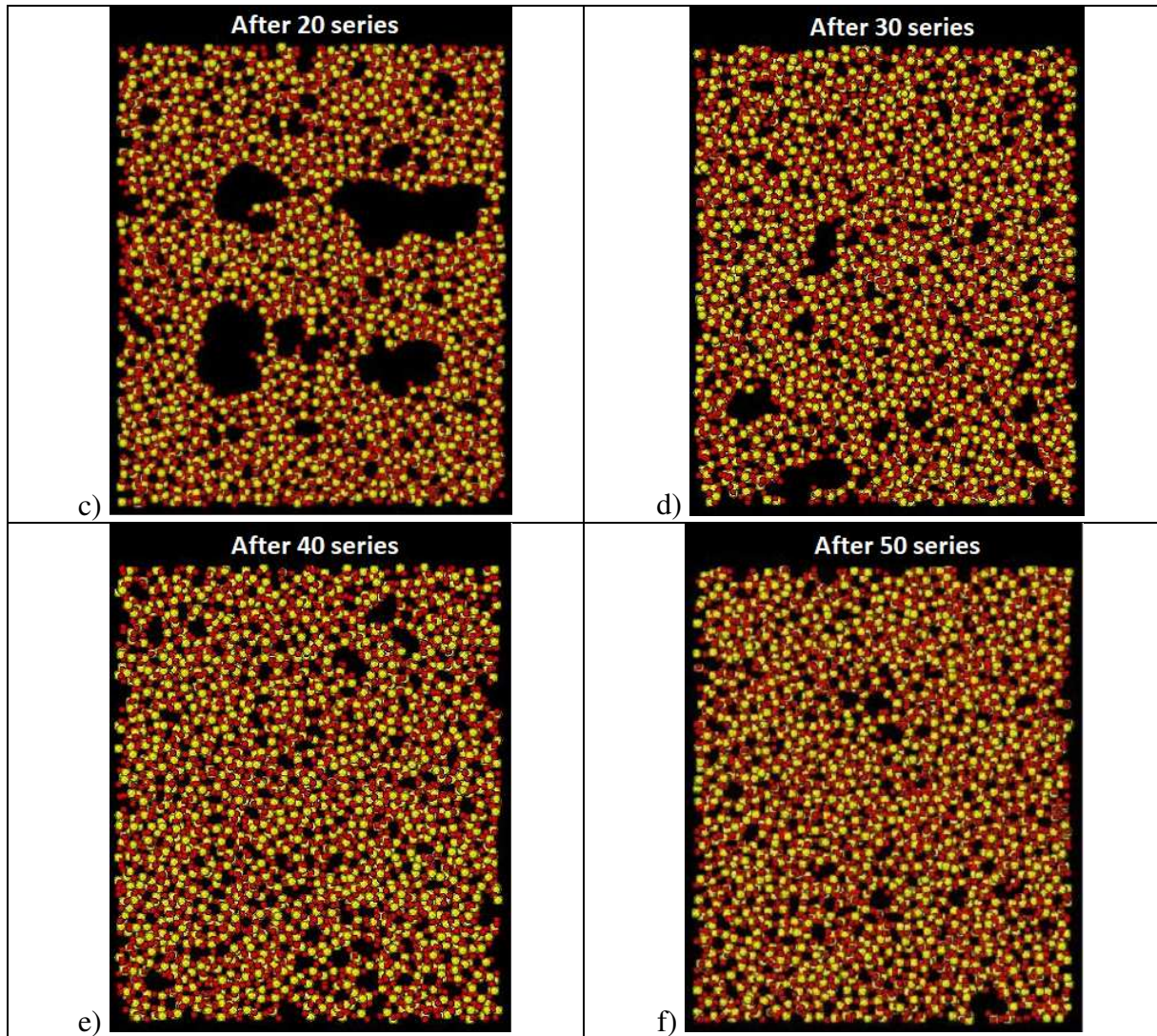

a) Initial state   b) After 10 series

Figure 5: 10Å thick slides a. before irradiation, b. after 10 series of 100 displacement cascades, c. after 20 series of 100 displacement cascades, d. after 30 series of 100 displacement cascades, e. after 40 series of 100 displacement cascades, f. after 50 series of 100 displacement cascades.

To confirm the dissolution of free volume within the bulk when the deposited energy increases, the following procedure has been followed. A set of 10000 random points have been drawn in the initial and final simulation cell and the distance between each of these points and the nearest "surface" atom (i.e. the atom characterized by a local free volume larger than the selected threshold) has been calculated. The distributions of these distances before and after 50 series of displacement cascades are plotted on Figure 6. Initially, there are less points close to the "surface" atoms and the tail shows that a significant quantity of points remains far from any "surface" atoms. After 50 series of displacement cascades, the quantity of points close to a "surface" atom increases drastically, and the tail disappears because free volume is present everywhere within the structure.
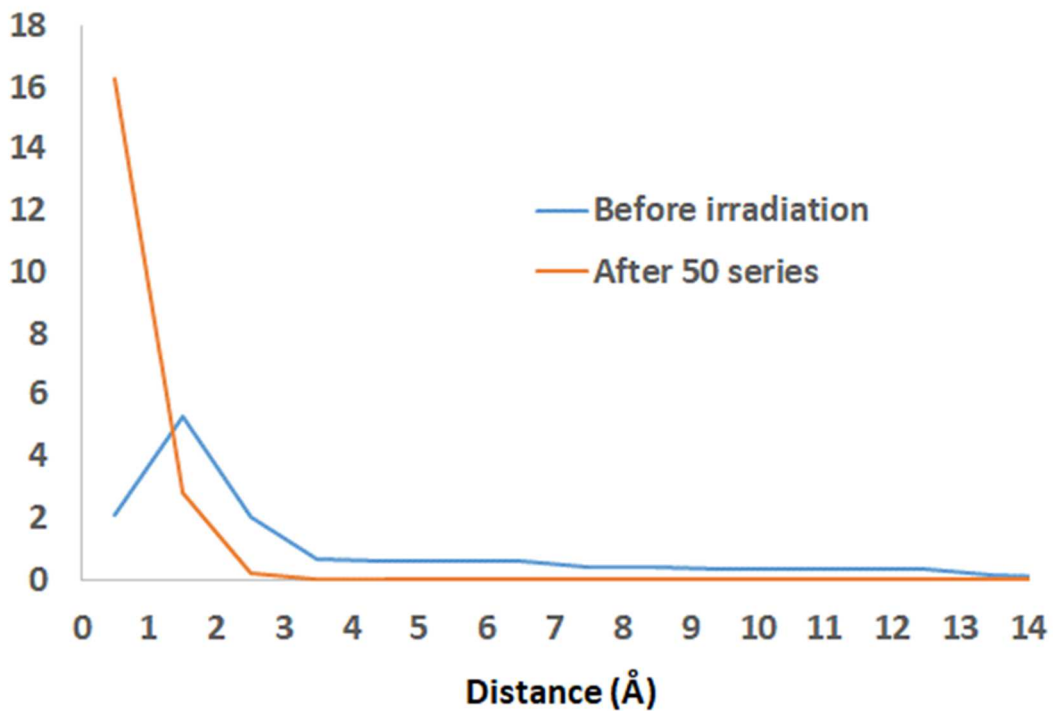
12

Figure 6. Nearest distance distributions between 10000 random points and the "surface" atoms before and after 50 series of displacement cascades. See the details in the text.

4. Characterization of the irradiated structures: Density

The density of the material was shown to increase during the accumulation of displacement cascades (see Figure 7). The silica continues to shrink after each series of displacement cascades and the shrinkage rate reaches a saturation plateau beyond 30 series displacement cascades. This threshold in the shrinkage rate is in agreement with what was observed on the atomic configurations and corresponds to the point of disappearance of mesopores (Figures 2 and 5) This result confirms that the stationary state is reached after roughly 30 series of 100 displacement cascades.
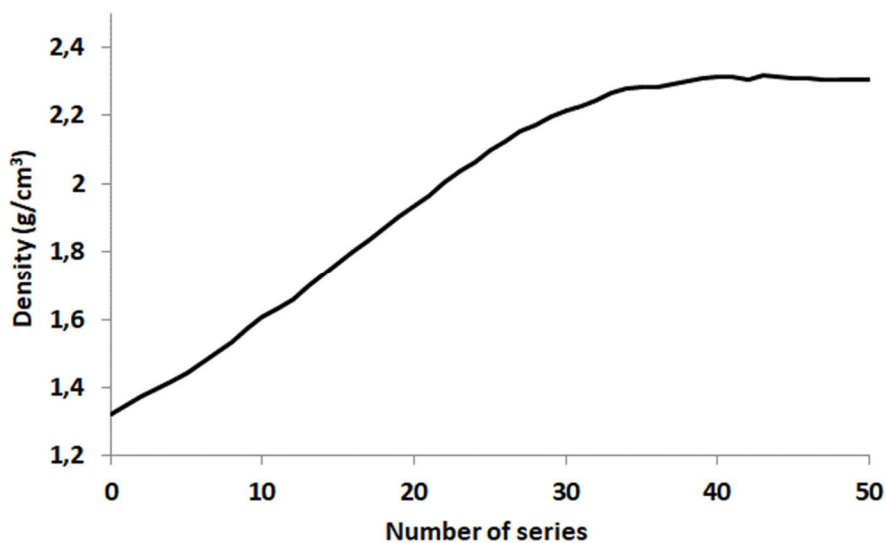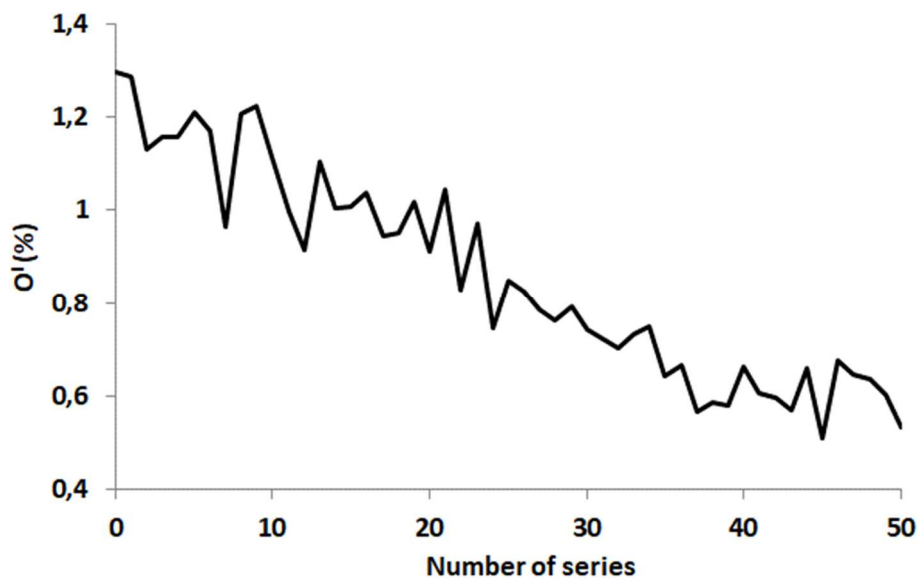
Figure 7: Density change versus the number of series of 100 displacement cascades.

5. Characterization of the irradiated structures: local coordination

The coordination of constituent atoms of the material have been calculated versus the deposited energy. The O^I, O^{II} and O^{III} atoms refer to one-, two-, and three-coordinate atoms. Similarly, the Si^{III}, Si^{IV} and Si^V atoms refer to three-, four-, and five-coordinate atoms. .
In the pristine structure, 197 O^I and 373 O^{III} were found. These atoms correspond to intrinsic defects formed during the creation of the initial porous structure.

Changes in the number of O^I and O^{III} are plotted as a function of the number of series of displacement cascades in Figure 8. The accumulation of displacement cascades induces a reduction in the number of the O^I atoms until the 30th series of displacement cascades, beyond which the number of O^I atoms reaches a plateau. This reduction in the number of O^I atoms is a result of the closure of the mesopores.
The result concerning the variation of the number of O^{III} atoms versus displacement cascade does not follow the same trend as their low-coordinate counterpart (i.e., O^I). During the first 30 series of 100 individual displacement cascades, the number of O^{III} decreases. After the removal of mesopores, the quantity of O^{III} increases and reaches a new stationary value. This observation has been attributed to the shrinkage of the bulk silica.
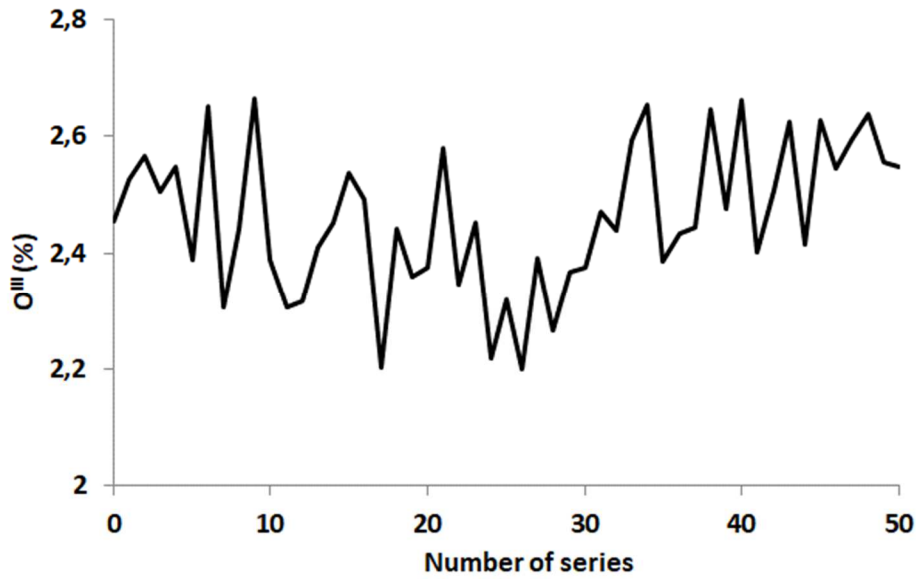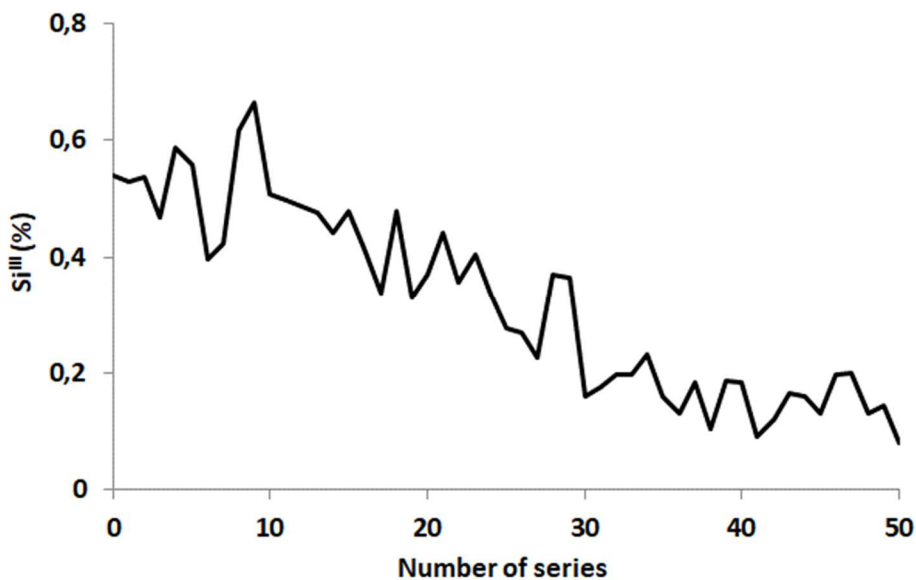
Figure 8. Top: Percentage of O^I versus the number of series of 100 individual cascades. Bottom: Percentage of O^{III} versus the number of series of 100 individual cascades.

Figure 9 shows the number of Si^{III} and Si^V versus the number of series of displacement cascades. Likewise, O^I atoms, the quantity of Si^{III} atoms continues to decrease until 30 series of displacement cascades before reaching a plateau.   This observation is due to the removal of the mesopores.

On the contrary, the quantity of Si^V atoms is stable until the 30th series and begins to increase beyond 30 series of displacement cascades. Likewise O^{III} atoms, this observation is also a result of the modification of the bulk silica.
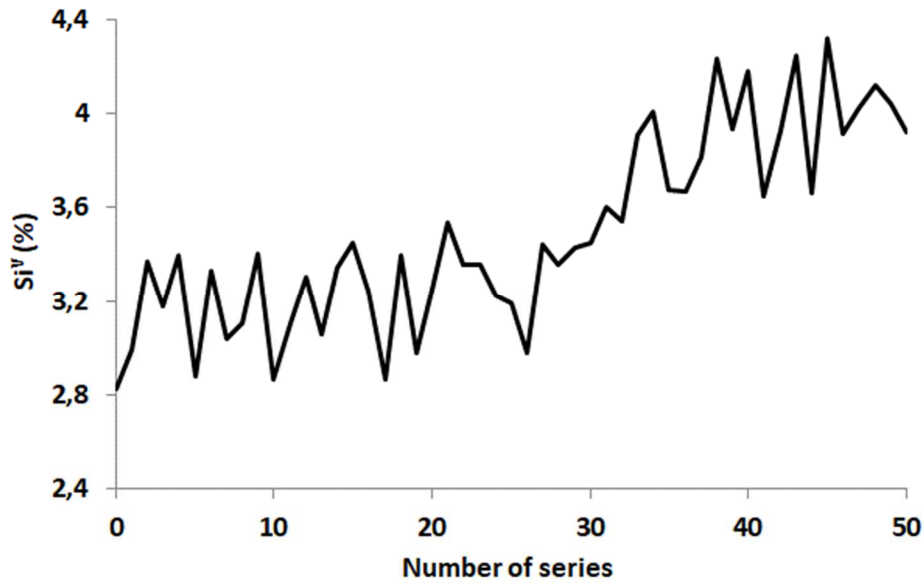
Figure 9. Top: Percentage of Si^{III} versus the number of series of 100 individual cascades. Bottom: Percentage of Si^{V} versus the number of series of 100 individual cascades.

6. Characterization of the irradiated structures: local angles

The Si-O-Si angular distributions have been measured before and after 10, 20, 30, 40 and 50 series of 100 displacement cascades (see Figure 10). Table II contains the average Si-O-Si angles within similar time frames.

Figure 10. Si-O-Si angular distributions before the irradiation and after 10, 20, 30, 40 and 50 series of 100 displacement cascades.

Two peaks can be observed from the plot of angular distributions with the small peak appearing around 98° and an intense broad peak around 143°. The first peak is most likely a result of the defects present in the initial structure.

During the accumulation of the displacement cascades, a slight increase of the average Si-O-Si angle occurs until a saturation plateau is reached as can be seen in Table II.

	Average Si-O-Si angle
Initially	143.46°
After 10 series of 100 displacement cascades	143.41°
After 20 series of 100 displacement cascades	143.86°
After 30 series of 100 displacement cascades	144.45°
After 40 series of 100 displacement cascades	144.77°
After 50 series of 100 displacement cascades	144.76°

Table II: Average Si-O-Si angle in the irradiated structures.

When bulk silica or more complex silicate glasses are subjected to a series of displacement cascades[29,34] a decrease in the average Si– O – Si bond angles is generally observed. However, in the present study we observe the opposite. To better understand the origin of this observation, we have plotted in Figure 11 the local volume of an O^{II} atom versus the local Si-O^{II}-Si angle (as said previously O^{II} means a twofold coordinated O atom) for the initial configuration and for the configuration subjected to 50 series of 100 displacement cascades. Only the twofold O atoms have been used because they belong to only one Si-O-Si bond.
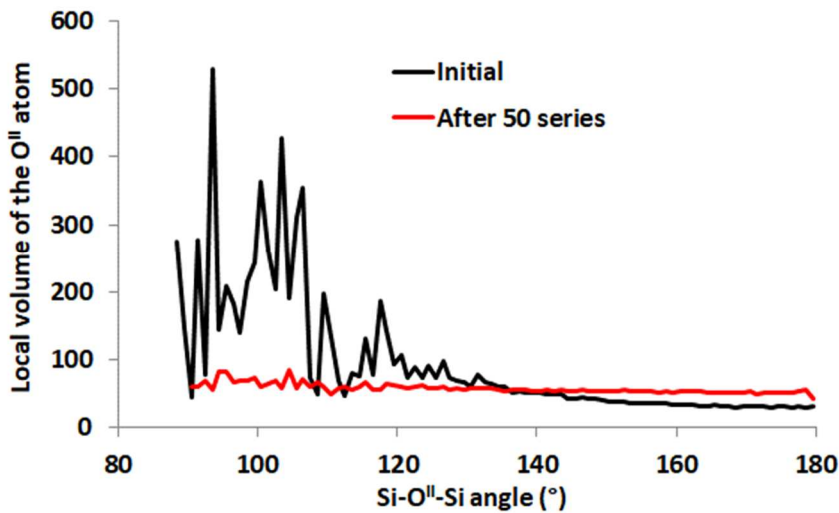

Figure 11. Average O local volume versus the Si-O-Si angle in the initial configuration and after 50 series of 100 displacement cascades. Only the two fold O atoms have been used. The local volume of an O^{II} atom is defined as the number of points closer to this atom as explained in the paragraph "Structural analyses of the irradiated structures". This corresponds to a volume in arbitrary units.

It can be seen from Figure 11 that the local volume of the O^{II} atom decreases with increasing Si-O-Si bond angle. As the pores continue to disappear during the accumulation of displacement cascades, the quantity of O^{II} atoms located at the surface of the pores decreases (as shown on Figure 4) and as a result, the average Si-O-Si bond angle is shifted towards larger values. This is confirmed quantitatively in Table III, wherein the average <Si-O-Si> bond angles for the "surface atoms" and "bulk atoms" in the initial structure and after 50 series of displacement cascades are provided. There is clearly an increase of the average <Si-O-Si> bond angles upon irradiation.

The low Si-O-Si angles associated to the O atoms located at the surface of the pores could be an artefact of the simulation because no atmosphere is considered here and the pores are

17

empty. In reality, gas molecules usually occupy the pores and hence the Si-O-Si bond angles at the surface of the pores could be quite different from the values predicted using simulation.

In addition, as can be seen in Figure 4, the atoms with a large local free volume are mainly located at the surface of the pores in the initial structure, but are much more dispersed after 50 series of displacement cascades. It means that in parallel to the removal of the pores, free volume is dissolved within the bulk. Using the definition of a "surface atom" given in the Research Method paragraph, we have indicated in Table III the average free volume (i.e. the number of points) around the O "surface atoms" and around the O "bulk atoms" in the pristine structure and after 50 series of displacement cascades.

	Initial structure	After 50 series of displacement cascades
<Si-O-Si> around the surface atoms	133.81	143.73
<Si-O-Si> around the bulk atoms	147.40	148.12
Volume around the O surface atoms	173.24	72.61
Volume around the O bulk atoms	32.55	47.24

Table III: Average <Si-O-Si> angles and free volumes around the O atoms (i.e. number of points around the O atoms, see Research Method paragraph) in the initial structure and after 50 series of 100 displacement cascades. The values for the "surface atoms" and "bulk atoms" are separated".

It can be seen that there is a large decrease of the free volume around the "surface atoms" and a significant increase of the free volume around the "bulk atoms". It means that the silica structure converges towards a more homogeneous one with bulk regions containing more free volume than before.

Discussion

1. Dimensional change - Comparison with experiments

The final objective of this study is to compare the volume change of the mesoporous silica thin film irradiated by 0.5 MeV Au ions with the results obtained from MD simulation. The comparison of these results is plotted in Figure 12 as a function of the energy deposited by ballistic effects (E_{bal}). The symmetry of the porous structure (cubic versus hexagonal) and the value of the energy for the incident projectile (U: 1.5 keV versus Au: 500 keV) are the main differences between the modelling and the experiment. Despite these differences, the observed trends are similar, based on the global density change, the mesoporous silica structure collapse completely for energies higher than 30 keV/nm^3. Unfortunately, we can't provide any information on the evolution of the porous volume which is another way to the densification, because even if this parameter is known for the simulated structure, X-Rays reflectometry doesn't allow the measurement of this parameter for the irradiated material.

To improve the agreement between the modelling and experiment, some factors should be taken into account while performing simulation and they are as follows: The modelling does not take into account the presence of surface silanol groups (-SiOH), while in experiments,

the silanol groups are present even after sintering at 500°C (as detected by infrared characterization). Such groups can influence the defect recombination at the pore surface thus affecting the final density of the material. The mesopores in experiment have hexagonal symmetry while in modelling they have cubic symmetry. Other potential reasons could also arise from the modelling method itself: i) the electronic effects of the irradiations are neglected, ii) an external cooling zone is added in order to simulate the heat dissipation process, iii) the boundary of the simulation box is completely free during relaxation process while in the experiment, the samples are constrained by the substrate, iv) the interatomic potentials are only approximations of the real force fields.
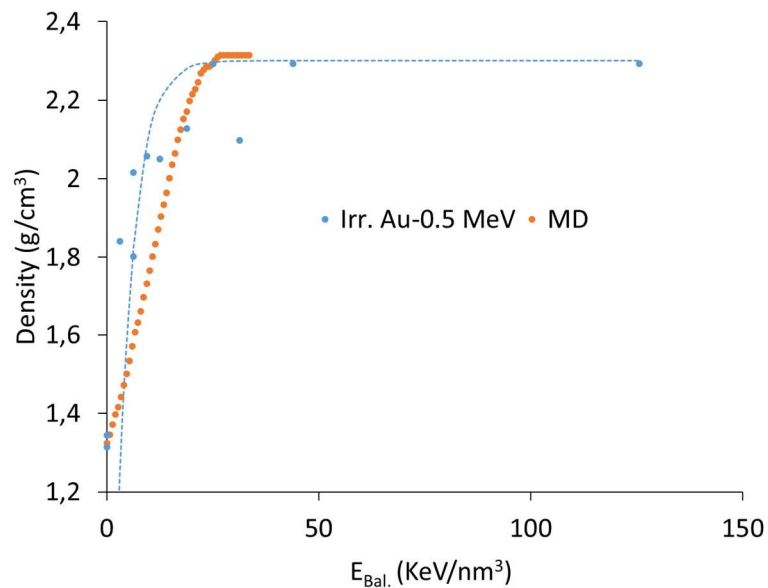

Figure 12. Comparison between experimental and modelling results. E_{bal} corresponds to the energy deposited by ballistic effects.

2. Pore collapse and densification process

As mentioned earlier, Molecular Dynamics simulations are in good agreement with the densification results observed experimentally during the irradiation of mesoporous thin films with Au-0.5MeV ions.

More precisely, it can be observed that the simulations of displacement cascades induce mainly local atomic displacements. A typical distribution of the atomic displacements during one displacement cascade is plotted in Figure 13 (insert). The large majority of individual displacements are lower than 2Å even if single individual displacements can reach 27Å (Figure 13). It means that the perturbations induced by the projectiles concern only the short-range order. In consequence, the progressive filling of the empty pores shown in Figure 3 is the consequence of local migrations of atoms located at the pore surfaces whose local environments have been disturbed during a series of atomic collisions. This process explains both the slow extinction of the pores and the progressive increase of the roughness at the pore surfaces.
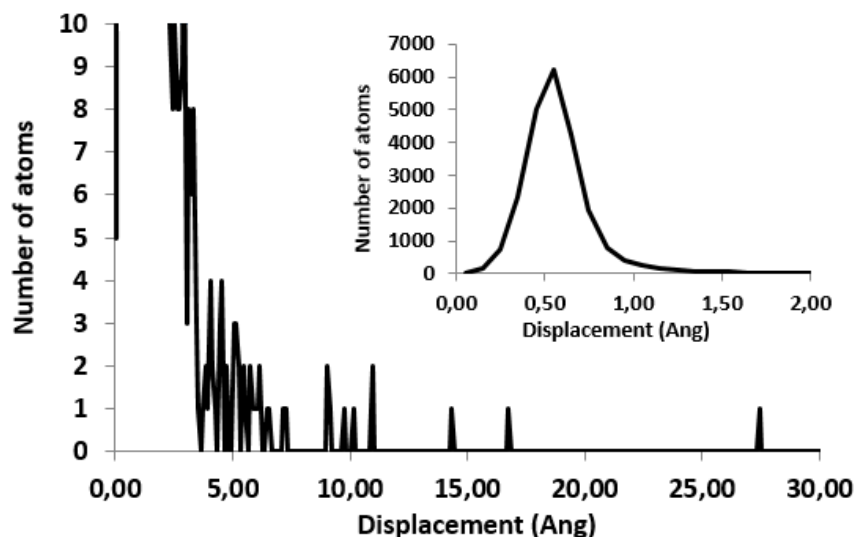
Figure 13. Tail up to 30Å of a typical atomic displacements distribution during one cascade. Insert: zoom on the distribution between 0 and 2Å.

It is however difficult to conclude on the physical phenomena of the origin of this densification. To provide a reasonable explanation, the authors consider the analogy between effects of irradiations and effect of thermal treatments on the mesoporous silica. Thermal treatment of thin films up to their densification can be likened to a sintering phenomenon. Little work has been done on the sintering of mesoporous silica's (film or bulk). Innocenzi[35] showed that the densification of this type of material starts from 600°C and that the total collapse of the structure is observed for a temperature higher than 900°C. We performed similar experiments and found a densification temperature comparable to that observed by Innocenzi. Evolutions of thin films after irradiation with Au-0.5MeV ions and thermal treatment were measured by XRR (Figure 14). The results indicate the same densification phenomenon: in both cases, the Bragg peaks are shifted towards the large angles, which means that the thickness of the pore-wall bilayer decreases. For a temperature above 900°C or a fluence higher than $7x10^{13}$, these peaks disappear indicating a complete densification of the structure. The analogies observed on the evolution of XRR diagrams versus temperature or fluence suggest a common origin. It is clear that in the case of sintering, the thermal diffusion associated to a decrease of the surface energy of the system is at the origin of the densification. It is well known that irradiation, especially in ballistic mode, accelerates atomic diffusion process[33]. Thus, the process of densification upon irradiation would be due to a low temperature diffusion of the atoms. Moreover, the MD modeling method only takes into account the effects of atomic displacements (i.e., diffusion) and makes it possible to reproduce the experiment. This result is also consistent with the hypothesis of "low temperature sintering" in relation with diffusion under irradiation.
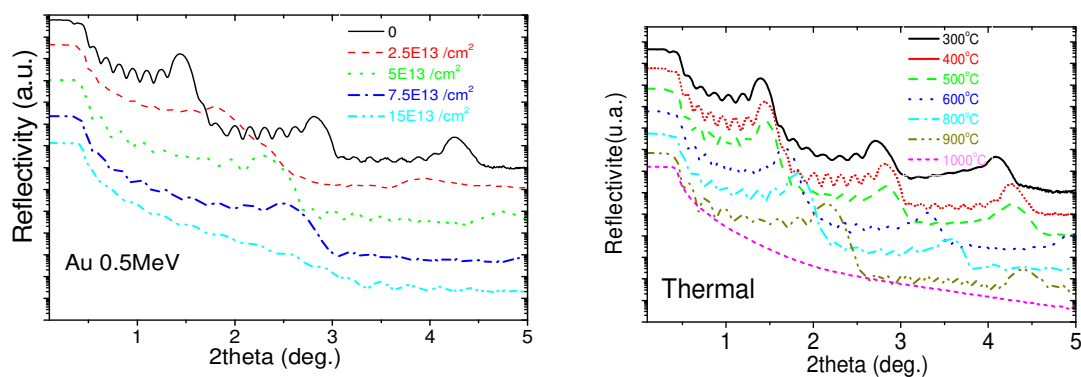
Figure 14. XRR curves of mesoporous silica thin films (a) irradiated at fluences from 0 to 15x10^{13} cm^{-2} by ions Au-0.5 MeV (b) heated at temperature from 300 to 1000°C.

Conclusion

The accumulation by molecular dynamics of cascades of U 1.2 keV in a mesoporous silica material having a cubic symmetry with a pore size 4 nm shows a complete collapse and densification of the structure for a ballistic deposited energy of 30 keV/nm^3. The final density of the sample, i.e. 2.3 g/cm^3, is slightly higher than the theoretical density of the amorphous silica. Simulation also shows that irradiation tends to close the mesopores leading to a glass structure with more free volume than initially.

The results obtained are in good agreement with the density evolution of mesoporous silica that were irradiated with Au ions (E=0.5 MeV). The differences observed can mainly be attributed to the difference in structures (hexagonal / cubic) of the materials studied, and to the fact that the modeling does not take into account the electronic effects associated with irradiation with gold ions.

The analogies between the density evolution of samples sintered at 1000°C and irradiated with gold ions (E=0.5 MeV) allow us to consider that a sintering mechanism under irradiation inducing ballistic displacements, could be the source of densification.

Acknowledgement

1.   Beck, J. S.; Vartuli, J. C.; Roth, W. J.; Leonowicz, M. E.; Kresge, C. T.; Schmitt, K. D.; Chu, C. T.

W.; Olson, D. H.; Sheppard, E. W.; McCullen, S. B.; Higgins, J. B.; Schlenker, J. L., A new family of

mesoporous molecular sieves prepared with liquid crystal templates. *Journal of the American*

Chemical Society 114, 10834-10843 (1992).

2.   Zhao, D.; Feng, J.; Huo, Q.; Melosh, N.; Fredrickson, G. H.; Chmelka, B. F.; Stucky, G. D., Triblock Copolymer Syntheses of Mesoporous Silica with Periodic 50 to 300 Angstrom Pores. *Science* 279, 548-552 (1998).

3.   (a) Sepehrian, H.; Ghannadi-Maragheh, M.; Waqif-Husain, S.; Yavari, R.; Khanchi, A. R., Sorption studies of radionuclides on a modified mesoporous cerium(IV) silicate. *Journal of Radioanalytical and Nuclear Chemistry* 275, 145-153 (2008); (b) Sepehrian, H.; Waqif-Husain, S.; Ghannadi-Maragheh, M., Development of Thiol-Functionalized Mesoporous Silicate MCM-41 as a Modified Sorbent and Its Use in Chromatographic Separation of Metal Ions from Aqueous Nuclear Waste. *Chromatographia* 70, 277-280 (2009).

4.   Corma, A., From Microporous to Mesoporous Molecular Sieve Materials and Their Use in Catalysis. *Chemical Reviews* 97, 2373-2420 (1997).

5.   Goettmann, F.; Moores, A.; Boissière, C.; Le Floch, P.; Sanchez, C., A Selective Chemical Sensor Based on the Plasmonic Response of Phosphinine-Stabilized Gold Nanoparticles Hosted on Periodically Organized Mesoporous Silica Thin Layers. *Small* 1, 636-639 (2005).

6.   Makowski, P.; Thomas, A.; Kuhn, P.; Goettmann, F., Organic materials for hydrogen storage applications: from physisorption on organic solids to chemisorption in organic molecules. *Energy & Environmental Science* 2, 480-490 (2009).

7.   Makowski, P.; Deschanels, X.; Grandjean, A.; Meyer, D.; Toquer, G.; Goettmann, F., Mesoporous materials in the field of nuclear industry: applications and perspectives. *New Journal of Chemistry* 36, 531-541 (2012).

8.   Duan, G.; Zhang, C.; Li, A.; Yang, X.; Lu, L.; Wang, X., Preparation and Characterization of Mesoporous Zirconia Made by Using a Poly (methyl methacrylate) Template. *Nanoscale Research Letters* 3, 118-122 (2008).

9.   Zhang, R.; Elzatahry, A. A.; Al-Deyab, S. S.; Zhao, D., Mesoporous titania: From synthesis to application. *Nano Today* 7, 344-366 (2012).

10.   (a) Klaumünzer, S., *Nucl. Instrum. Methods B* 166, 459-464 (2000); (b) Klaumünzer, S., *Nucl. Instrum. Methods B* 191, 356-361 (2002).

11.   S. Dourdain, X. D., G. Toquer, C. Grygiel, I. Monnet, S. Pellet-Rostaing, A. Grandjean, *J. Nucl. Mater.* 427, 411 (2012).

12.   Lou, Y.; Toquer, G.; Dourdain, S.; Rey, C.; Grygiel, C.; Simeone, D.; Deschanels, X., Structure evolution of mesoporous silica SBA-15 and MCM-41 under swift heavy ion irradiation. *Nuclear Instruments and Methods in Physics Research Section B: Beam Interactions with Materials and Atoms Part A* 365, 336-341 (2015).

13.   Kucheyev, S. O.; Hamza, A. V.; Worsley, M. A., Ion-beam-induced stiffening of nanoporous silica. *Journal of Physics D: Applied Physics* 42, 182003 (2009).

14.   Kucheyev, S. O.; Wang, Y. M.; Hamza, A. V.; Worsley, M. A., Light-ion-irradiation-induced thermal spikes in nanoporous silica. *Journal of Physics D: Applied Physics* 44, 085406 (2011).

15.   (a) Beyerlein, I. J.; Caro, A.; Demkowicz, M. J.; Mara, N. A.; Misra, A.; Uberuaga, B. P., Radiation damage tolerant nanomaterials. *Materials Today* 16, 443-449 (2013); (b) Sun, C.; Bufford, D.; Chen, Y.; Kirk, M. A.; Wang, Y. Q.; Li, M.; Wang, H.; Maloy, S. A.; Zhang, X., In situ study of defect migration kinetics in nanoporous Ag with enhanced radiation tolerance. *Scientific Reports 4*, 3737 (2014).

16.   Bringa, E. M.; Monk, J. D.; Caro, A.; Misra, A.; Zepeda-Ruiz, L.; Duchaineau, M.; Abraham, F.; Nastasi, M.; Picraux, S. T.; Wang, Y. Q.; Farkas, D., Are Nanoporous Materials Radiation Resistant? *Nano Letters* 12, 3351-3355 (2012).

17.   Li, J.; Wang, H.; Zhang, X., A Review on the Radiation Response of Nanoporous Metallic Materials. 70, 2753-2764 (2018).

18.   Lou, Y.; Dourdain, S.; Rey, C.; Serruys, Y.; Simeone, D.; Mollard, N.; Deschanels, X., Structure evolution of mesoporous silica under heavy ion irradiations of intermediate energies. *Microporous and Mesoporous Materials* 251, 146-154 (2017).

19.   Manzini, A. M.; Alurralde, M. A.; Giménez, G.; Luca, V., The radiation response of mesoporous nanocrystalline zirconia thin films. *Journal of Nuclear Materials* 482, 175-186 (2016).

20.   Anders, C.; Bringa, E. M.; Urbassek, H. M., Sputtering of a metal nanofoam by Au ions. *Nuclear Instruments & Methods in Physics Research Section B-Beam Interactions with Materials and Atoms* 342, 234-239 (2015).

21.   Sycheva, A. A.; Voronina, E. N.; Rakhimova, T. V.; Rakhimov, A. T., Influence of porosity and pore size on sputtering of nanoporous structures by low-energy Ar ions: Molecular dynamics study. *Applied Surface Science* 475, 1021-1032 (2019).

22.   Siboulet, B.; Coasne, B.; Dufrêche, J.-F.; Turq, P., Hydrophobic Transition in Porous Amorphous Silica. *The Journal of Physical Chemistry B* 115, 7881-7886 (2011).

23.   van Beest, B. W. H.; Kramer, G. J.; van Santen, R. A., Force fields for silicas and aluminophosphates based on \textit{ab initio} calculations. *Physical Review Letters* 64, 1955-1958 (1990).

24.   Wootton, A.; Thomas, B.; Harrowell, P., Radiation-induced densification in amorphous silica: A computer simulation study. *Journal of Chemical Physics 115*, 3336-3341 (2001).

25.   Mota, F.; Caturla, M. J.; Perlado, J. M.; Dominguez, E.; Kubota, A., Atomistic simulations of threshold displacement energies in SiO2. *MRS Proceedings* 792 *(2003)*.

26.   Trachenko, K.; Dove, M. T.; Artacho, E.; Todorov, I. T.; Smith, W., Atomistic simulations of resistance to amorphization by radiation damage. *Physical Review B* 73, 174207 (2006).

27.   Trachenko, K.; Zarkadoula, E.; Todorov, I. T.; Dove, M. T.; Dunstan, D. J.; Nordlund, K., Modeling high-energy radiation damage in nuclear and fusion applications. *Nuclear Instruments and Methods in Physics Research Section B: Beam Interactions with Materials and Atoms* 277, 6-13 (2012).

28.   Zhen, J. S.; Yang, Q.; Yan, Y. H.; Jiang, X. W.; Yan, S. A.; Chen, W.; Guo, X. Q., Molecular dynamics study of structural damage in amorphous silica induced by swift heavy-ion radiation. *Radiation Effects and Defects in Solids* 171, 340-349 (2016).

29. Delaye, J. M.; Peuget, S.; Bureau, G.; Calas, G., Molecular dynamics simulation of radiation damage in glasses. *Journal of Non-Crystalline Solids* 357, 2763-2768 (2011).

30. Todorov I.T., Smith W., Trachenko K., Dove M.T., DL_POLY_3: new dimensions in molecular dynamics simulations via massive parallelism. *Journal of Materials Chemistry* 16, 1911-1918 (2006).

31. Ziegler, J.; Biersack, J.; Littmark, U.; The stopping power and ranges of ions in matter. Vol. I, Pergamon, New York, **1985**.

32. Ziegler, J. F.; Biersack, J. P., TRIM/SRIM 2013.

33. Martin, G., Phase-stability under irradiation – ballistic effects. *Physical Review B* 30, 1424-1436 (1984).

34. Delaye, J.-M.; Peuget, S.; Bureau, G.; Calas, G.; *Journal of Non-Crystalline Solids* 357, 2763-2768 (2011).

35. Innocenzi, P.; Falcaro, P.; Grosso, D.; Babonneau, F., Order-disorder transitions and evolution of silica structure in self-assembled mesostructured silica films studied through FTIR spectroscopy. *Journal of Physical Chemistry B* 107, 4711-4717 (2003).